J|A|C|S
ARTICLES
Published on Web 10/06/2007

Spatial and Intensity Modulation of Nanowire Emission Induced by Mobile Charges

Vladimir Protasenko,[†] Stanislav Gordeyev,[‡] and Masaru Kuno*,[†]

Contribution from the Department of Chemistry and Biochemistry, Notre Dame Radiation Laboratory and Department of Aerospace and Mechanical Engineering, University of Notre Dame, Notre Dame, Indiana 46556

Received June 4, 2007; E-mail: mkuno@nd.edu

Abstract: Single-molecule optical experiments carried out in conjunction with externally applied electric fields show deliberate spatial and intensity control over CdSe nanowire (NW) emission. In particular, by applying external fields to electrically isolated (single) NWs, their emission can be localized in areas of the wire closest to the positive electrode. In a few cases, the resulting emission intensity increases over the corresponding zero-field value by nearly an order of magnitude. More often than not, factors of 2−3 are seen. Reversing the field polarity causes the emission to localize in opposite regions of the wire. Emission from individual NWs can therefore be modulated. Complementary ac electric field measurements show that the effect persists up to 500 kHz. To explain the phenomenon, the effective passivation of surface trap states by mobile carriers is speculated. This, in turn, causes local changes in the NW emission quantum yield (QY). To verify the presence of such mobile charges, both ensemble and single NW bundle electrophoresis experiments are conducted. By investigating subsequent NW rotational and translational dynamics, an estimate for the number of mobile carriers is determined. A lower limit (best case) linear charge density of ∼0.45−1.2 mobile electrons per micrometer of the wire is obtained. Apart from self-consistently explaining the field-induced NW emission modulation, the resulting data and subsequent analysis also suggests that the same mobile carriers may be the root cause of NW emission intermittency. Furthermore, given the ubiquity of stray charges, the resulting hypothesis may have additional applicability toward explaining blinking in other systems, a problem of current interest especially within the context of colloidal QDs.

Introduction

Mobile or static charges can significantly alter the physical, chemical, and optical/electrical properties of metal, semiconductor, and dielectric particles. This is especially true when the particle size falls below a micrometer given concurrent increases in the particle surface to volume ratio. Millikan was one of the first to observe such size-dependent properties having analyzed the trajectories of micrometer-sized oil droplets subjected to an external electric field.[1]

Charges on nanoparticles (NPs) have since been utilized in countless studies and applications. For example, the simplest use of surface charges is the electrostatic stabilization of colloidal suspensions.[2] In this respect, Faraday's colloidal gold sols can still be seen at the Royal Institution of Great Britain.[3] More recently the controlled electrophoretic deposition of smooth CdSe quantum dot [QD, also called nanocrystals, (NCs)] films, as well as their mixtures with other NPs, has been reported. This opens up new ways for manufacturing nanostructured devices.[4] Furthermore, electrostatic forces between charged nanocrystals dictate their assembly into complex three-dimensional colloidal crystals, possessing potentially unique collective properties.[5,6]

Charges and associated electric fields alter not only the self-assembly or electrophoretic motion of nanoparticles but also modify their optical[7−12] and electrical[13,14] properties. In the case of colloidal QDs, both their fluorescence intensity and spectral position are influenced by the presence of mobile charges. Specifically, carriers migrating on a NC surface produce

[†] Notre Dame Radiation Laboratory.
[‡] Department of Aerospace and Mechanical Engineering.

(1) Millikan, R. A. *Nobel Lectures, Physics 1922−1941*; Elsevier Publishing Co.: Amsterdam, 1965.
(2) Hunter, R. J. *Foundation of colloid science*; Oxford Science Publication, Clarendon Press: Oxford, 1991; Vol. 1.
(3) Tweney, R. D. *Perspect. Sci.* **2006**, *14*, 97−121.
(4) Islam, M. A.; Xia, Y.; Telesca, D. A., Jr.; Streigerwald, M. L.; Herman, I. P. *Chem. Mater.* **2004**, *16*, 49−54. Islam, M. A.; Xia, Y.; Steigerwald, M. L.; Yin, M.; Liu, Z.; O'Brien, S.; Levicky, R.; Herman, I. P. *Nano Lett.* **2003**, *3*, 1603−1606. Islam, M. A.; Herman, I. P. *Appl. Phys. Lett.* **2002**, *80*, 3823−3825.
(5) Shevchenko, E. V.; Talapin, D. V.; Kotov, N. A.; O' Brien, S.; Murray, C. B. *Nature* **2006**, *439*, 55−59.
(6) Klajn, R.; Bishop, K. J. M.; Fialkowski, M.; Paszewski, M.; Campbell, C. J.; Gray, T. P.; Grzybowski, B. A. *Science* **2007**, *316*, 261−264. Kalsin, A. M.; Fialkowski, M.; Paszewski, M.; Smoukov, S. K.; Bishop, K. J. M.; Grzybowski, B. A. *Science* **2006**, *312*, 420−424. Kalsin, A. M.; Pinchuk, A. O.; Smoukov, S. K.; Paszewski, M.; Schatz, G. C.; Grzybowski, B. A. *Nano Lett.* **2006**, *6*, 1896−1903.
(7) Pokutnyi, S. I.; Jasak, L.; Misiewicz, J.; Salejda, W.; Zegrya, G. G. *J. Appl. Phys.* **2004**, *96*, 1115−1119.
(8) Blanton, S. A.; Hines, M. A.; Guyot-Sionnest, P. *Appl, Phys. Lett.* **1996**, *69*, 3905−3907.
(9) Empedocles, S. A.; Bawendi, M. G. *Science* **1997**, *278*, 2114−2117.
(10) Neuhauser, R. G.; Shimizu, K. T.; Woo, W. K.; Empedocles, S. A.; Bawendi, M. G. *Phys. Rev. Lett.* **2000**, *85*, 3301−3304.
(11) Efros, Al. L.; Rosen, M. *Phys. Rev. Lett.* **1997**, *78*, 1110−1113.

10.1021/ja073642w CCC: $37.00

sufficiently strong electric fields to cause time-dependent spectral changes as well as increases in line width.[8−10] These Stark-induced shifts are accompanied by abrupt jumps of the fluorescence intensity believed to be caused by sequential QD ionization and neutralization events. The phenomenon is often referred to as "blinking" and remains distinct from triplet-induced quantum jumps.[11,12] Spectral shifts, line broadening, and fluorescence intermittency are also observed in semiconductor nanorods (NRs) and arise for similar reasons.[15]

When nanostructures evolve from zero-dimensional (0D) QDs to one-dimensional (1D) NWs, the lowering of the overall structural symmetry impacts the material's optical and electrical properties. This leads to unique 1D phenomena. For example, radial confinement of electrons and holes modifies the nanostructure's joint density of states. Moreover, valence band mixing occurs, inducing variations in subband oscillator strength as well as introducing intrinsic polarization anisotropies.[16] Differences in NW/local environment dielectric constants also significantly alter exciton binding energies, suggesting possible dielectric contrast "engineering" of 1D nanostructures.[17]

Corresponding differences in 1D optical and electrical properties are also expected when NRs and NWs are in the presence of mobile charges. Specifically, in the limiting case of NWs, we observe the appearance of unexpected optical effects such as field-induced fluorescence enhancement,[18] intrawire fluorescence intensity, and spectral heterogeneity, as well as spatially correlated intensity fluctuations.[19] These effects likely stem from the presence of excess surface charges. When studies of these properties are combined with the unique structural asymmetries of NWs, new insights into these ubiquitous, yet unexplained, optical phenomena are possible.

In the experiments described below we show in detail the spatial and intensity modulation of single NW emission when in the presence of external electric fields. In particular, we demonstrate that the NW emission becomes localized in regions of the structure closest to the positive electrode. A corresponding emission quenching of near identical magnitude occurs at the opposite end. When the polarity of the electric field is reversed, previously dark regions of the NW become bright. The NW emission can therefore be spatially "toggled". In all cases, emission enhancements (quenchings) of 2−3 times are seen with occasional order of magnitude changes. Complementary ac electric field measurements show that the effect persists up to 500 kHz, limited by the bandwidth of the electronics.

Because the emission enhancement always occurs near the positive electrode, we suggest that mobile electrons in or on the NW are responsible for the phenomenon. To verify and quantify their associated linear charge density, direct electrophoresis experiments of NWs dispersed in toluene, chloroform, immersion oil, and oleic acid were conducted. Analyses of NW rotational and translational dynamics show that mobile charges indeed exist on or within the wire. Multiple contributions to these charges exist, stemming from both extrinsic and photogenerated sources.

This manuscript is structured as follows. We first describe experimental details of optical experiments using external electric fields showing both the spatial and intensity modulation of the NW emission. We then present results from translational and rotational electrophoresis experiments carried out on both NW ensembles and small bundles of individual wires. A simple model for their rotational and translational dynamics is then used to verify as well as quantify the associated linear charge density. Finally, we posit why such mobile carriers may impact the optical and electrical properties of NWs as well as their dynamics. Furthermore, we speculate that such mobile charges may play a crucial role in dictating the fluorescence intermittency of other systems such as colloidal QDs.

Experimental Section

Synthesis. Narrow diameter CdSe NWs were prepared using a seeded solution approach described previously.[20] Briefly, low-melting bimetallic Au/Bi nanoparticles are made by overcoating Au seed particles (1.5 nm diameter) with elemental bismuth. The overcoating procedure entails adding $BiEt_3$ to Au NPs dispersed in trioctylphosphine and phenyl ether at mild temperatures on the order of 100 °C. Resulting bimetallic particles have diameters ranging from 1.4 to 3.0 nm with a corresponding size distribution of ∼20%.[21]

Controlled amounts of these "catalyst" NPs are then introduced along with trioctylphosphine selenide (TOPSe) into a mixture of Cd ions coordinated with fatty or phosphonic acids. The current synthesis employs octanoic acid, although oleic acid may be used as well.[22] The high-boiling coordinating solvent is trioctylphosphine oxide (TOPO). As such, the overall reaction is nearly identical to the synthesis of analogous colloidal CdSe QDs.[23]

A typical reaction consists of mixing 2.5 g (6.47 mmol) of TOPO, 25 mg (0.194 mmol) of CdO, and 0.23 mL (1.43 mmol) of octanoic acid. The resulting mixture is heated until clear at which point 25 μL of 1 M TOPSe (25 μmol) and ∼230 μL of the Au/Bi stock are introduced. This yields a rapid color change indicating NW growth.

Depending upon the amount of excess surfactant present, the wires are soluble in common organic solvents such as toluene or chloroform. They can be precipitated from solution using polar solvents such as methanol, ethanol, and isopropyl alcohol. As such, the wires can be "washed" multiple times to remove any excess surfactant.

HRTEM Characterization. Survey TEM experiments were conducted using a JEOL JEM-100SX microscope. Actual low- and high-resolution TEM micrographs were taken with a JEOL-2010 TEM

(12) Kuno, M.; Fromm, D. F.; Hamann, H. F.; Gallagher, A.; Nesbitt, D. J. *J. Chem. Phys.* **2000**, *112*, 3117. Kuno, M.; Fromm, D. F.; Hamann, H. F.; Gallagher, A.; Nesbitt, D. J. *J. Chem. Phys.* **2001**, *115*, 1028. Kuno, M.; Fromm, D. F.; Gallagher, A.; Nesbitt, D. J.; Micic, O. I.; Nozik, A. J. *Nano Lett.* **2001**, *1*, 557. Kuno, M.; Fromm, D. F.; Johnson, S. T.; Gallagher, A.; Nesbitt, D. J. *Phys. Rev. B* **2003**, *67*, 125304.
(13) Maenosono, S. *Chem. Phys. Lett.* **2003**, *376*, 666−670. Uematsu, T.; Maenosono, S.; Yamaguchi, Y. *J. Phys. Chem. B* **2005**, *109*, 8613−8618. Atsushi A.; Maenosono, S. *J. Chem. Phys.* **2006**, *125*, 114705. Uematsu, T.; Maenosono, S.; Yamaguchi, Y. *Appl. Phys. Lett.* **2006**, *89*, 031910. Kimura, J.; Uematsu, T.; Maenosono, S.; Yamaguchi, Y. *J. Phys. Chem. B* **2004**, *108*, 13258−13264.
(14) Patolsky, F.; Zheng, G.; Hayden, O.; Lakadamyali, M.; Zhuang, X.; Lieber, C. *PNAS* **2004**, *101*, 14017−14022.
(15) Muller, J.; Lupton, J. M.; Rogach, A. L.; Feldmann, J.; Talapin, D. V.; Weller, H. *Phys. Rev. B* **2005**, *72*, 205339. Muller, J.; Lupton, J. M.; Rogach, A. L.; Feldmann, J.; Talapin, D. V.; Weller, H. *Phys. Rev. Lett.* **2004**, *93*, 167402.
(16) Palmgren, S.; Weman, H.; Schoenberg, A.; Karlsson, K. F.; Dupertuis, M. A.; Leifer, K.; Ruda, A.; Kapon, E. *Appl. Phys. Lett.* **2006**, *89*, 191111. Vouilloz, F.; Oberli, D. Y.; Dupertuis, M. A.; Gustafsson, A.; Reinhardt, F.; Kapon, E. *Phys. Rev. B* **1998**, *57*, 12378. Vouilloz, F.; Oberli, D. Y.; Dupertuis, M. A.; Gustafsson, A.; Reinhardt, F.; Kapon, E. *Phys. Rev. Lett.* **1997**, *78*, 1580.
(17) Muljarov, E. A.; Zhukov, E. A.; Dneprovskii, V. S.; Masumoto, Y. *Phys. Rev. B* **2000**, *62*, 7420−7432.
(18) Zhou, R.; Chang, H.-C.; Protasenko, V.; Kuno, M.; Singh, A. K.; Jena, D.; Xing, H. *J. Appl. Phys.* **2007**, *101*, 073704.
(19) Protasenko, V. V.; Hull, K.; Kuno, M. *Adv. Mater.* **2005**, *17*, 2942−2949.
(20) Grebinski, J. W.; Hull, K. L.; Zhang, J.; Kosel, T. H.; Kuno, M. *Chem. Mater.* **2004**, *16*, 5260−5272.
(21) Grebinski, J. W.; Richter, K. L.; Zhang, J.; Kosel, T. H.; Kuno, M. *J. Phys. Chem. B* **2004**, *108*, 9745−9751.
(22) Wang, F.; Dong, A.; Sun, J.; Tang, R.; Buhro, W. *Inorg. Chem.* **2006**, *45*, 7511−7521.
(23) Peng, Z. A.; Peng, X. *J. Am. Chem. Soc.* **2001**, *123*, 183−184.

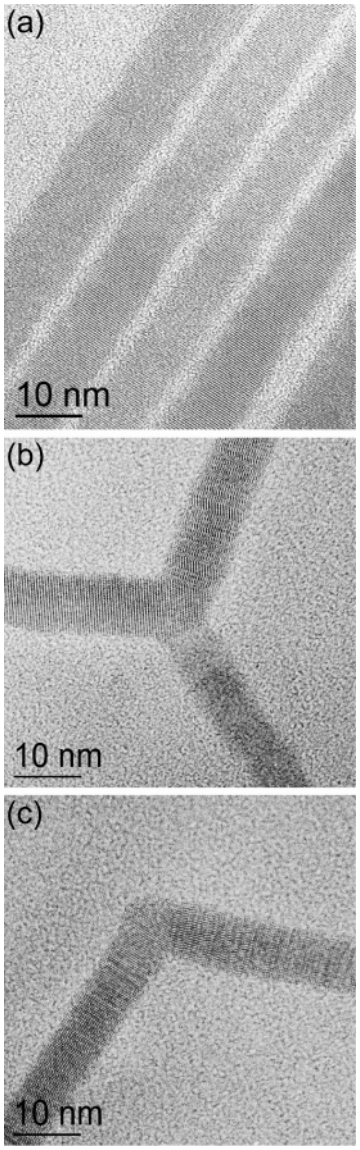

Figure 1. High-resolution TEM images of (a) straight, (b) tripod, and (c) v-shaped CdSe NWs.

operating at 200 kV. Dilute NW solutions in toluene or chloroform were dropped onto ultrathin carbon TEM grids (Ladd) and allowed to dry. Resulting high-resolution TEM micrographs shown in Figure 1 confirm NW diameters between 5 and 12 nm. These values are below twice the bulk exciton Bohr radius of CdSe, and as such confinement effects may be expected. The wires also have large aspect ratios (lengths between 1 and 10 μm), narrow diameter distributions (20−30%), and corresponding intrawire variations of 3−6%. Examination of <110>-oriented NWs reveals zinc blende/wurtzite sectioning along their length. By varying the metal/chalcogen stoichiometry as well as the NW growth temperature, branched wires with characteristic tripod, v-shape, y-shape, and "merge-y" morphologies can be obtained (Figure 1b and 1c).[20]

Optical Instrumentation. Emission experiments were conducted using a modified, single-molecule imaging instrument built around a Nikon Eclipse TE2000-U inverted optical microscope. An air-cooled Ar^+ ion laser (Melles Griot) provides the 488 nm (2.54 eV) excitation. Its output is first dispersed through a prism and subsequently spatially filtered to remove any plasma light or extraneous laser lines. After being attenuated with a series of neutral density filters, the light is coupled into a single-mode, polarization preserving optical fiber. The transmitted light is then collected and collimated with an infinity corrected objective (Olympus, resulting beam diameter $\approx$ 10 mm). The light's polarization is made circular through a quarter wave plate. If needed, it is made linear using a sheet polarizer. All experiments are conducted with circularly polarized light unless otherwise stated. Under epi-illumination conditions, the light is focused prior to the microscope objective (Nikon 60×/1.40 oil immersion) with a +400 mm focal length achromat. A 20−30 μm diameter spot results on the sample. Corresponding excitation intensities are $\sim$150 W/cm^2. Any sample emission is collected with the same microscope objective and is passed through two barrier filters (Chroma) prior to being imaged on a CCD (DVC) attached to an imaging spectrometer (Acton).

Electric Field Measurements. Interdigitated metal electrodes on glass cover slips were fabricated using standard photolithographies involving PMMA deposition, exposure through a mask, and etching with developer. A thin ($\sim$5 nm) Ti buffer layer is deposited on the substrate to act as a gold adhesion layer. Approximately 100 nm of Au is then added to create 20−100 μm gap electrodes. Subsequent liftoff is performed in acetone.

Samples are mounted on a closed loop piezo stage (Physik Instrumente). This enables accurate alignment of single NWs at the center of our excitation spot where the intensity profile is most uniform. A function generator (Tektronix) along with a 20× amplifier provides voltages to the interdigitated electrodes through a home-built probe station. Tapered tungsten wires are used as probes. Typical frequencies of the applied stepwise voltage vary from 0.01 Hz to 500 kHz with the high-frequency limit determined by the amplifier bandwidth.

In electric field experiments, samples were prepared by drop-casting NWs from dilute solutions in toluene onto premade glass cover slips with electrodes. Field-modulated images are collected from individual (electrically isolated) NWs. Specifically, the majority of our experiments are carried out on branched wires with characteristic tripod, v-shape, y-shape, and merge-y morphologies. This is because complementary TEM experiments show these specimens to be predominantly single wires. Complications associated with imaging small bundles of straight NWs are therefore avoided. Occasionally, straight wires with uniform emission intensities and magnitudes are used. The 20−100 μm gap between electrodes provides sufficient room to locate wires situated at least a few micrometers away from either Au contact, preventing any charge-transfer effects. Electric field measurements are carried out on NWs residing at the air/glass interface.

Microelectrophoresis. The same optical instrument is used for microelectrophoresis experiments. To conduct these studies, substrates consisting of glass cover slips with microcavities glued to their top were built (Figure S1, Supporting Information). A deep, narrow slot is present between the electrodes to minimize any edge effects and to ensure subsequent field uniformity. Experiments are conducted with electric field amplitudes between 500 V/cm and 2 kV/cm and with NWs dispersed in either immersion oil or oleic acid.

Microcavities were constructed by cleaving 0.5−0.6 mm thick pieces of silicon and coating them with 50 nm of Au using a sputter coater (Emitech). Small 4 × 4 to 6 × 6 mm^2 sections were then glued to the cover slip using 5 min epoxy. A small $\sim$100 μm thick piece of paper is placed between the electrodes to define their spacing. This shim is subsequently removed once the glue has cured. Gold wires ($\sim$60 μm diameter) are then attached to the electrodes using conductive epoxy and also connected to the above voltage source. To stabilize NW solutions inside the gap and prevent any unwanted drift, the microcavity is surrounded by a small perfusion chamber.

Results and Discussion

Electric Field Modulation of the NW Emission. Optical experiments conducted on individual (electrically isolated) NWs in the presence of external electric fields show unexpected behavior. Namely, the emission from each NW localizes in regions of the wire closest to the positive electrode. This is accompanied by a noticeable (2−3-fold) enhancement of the

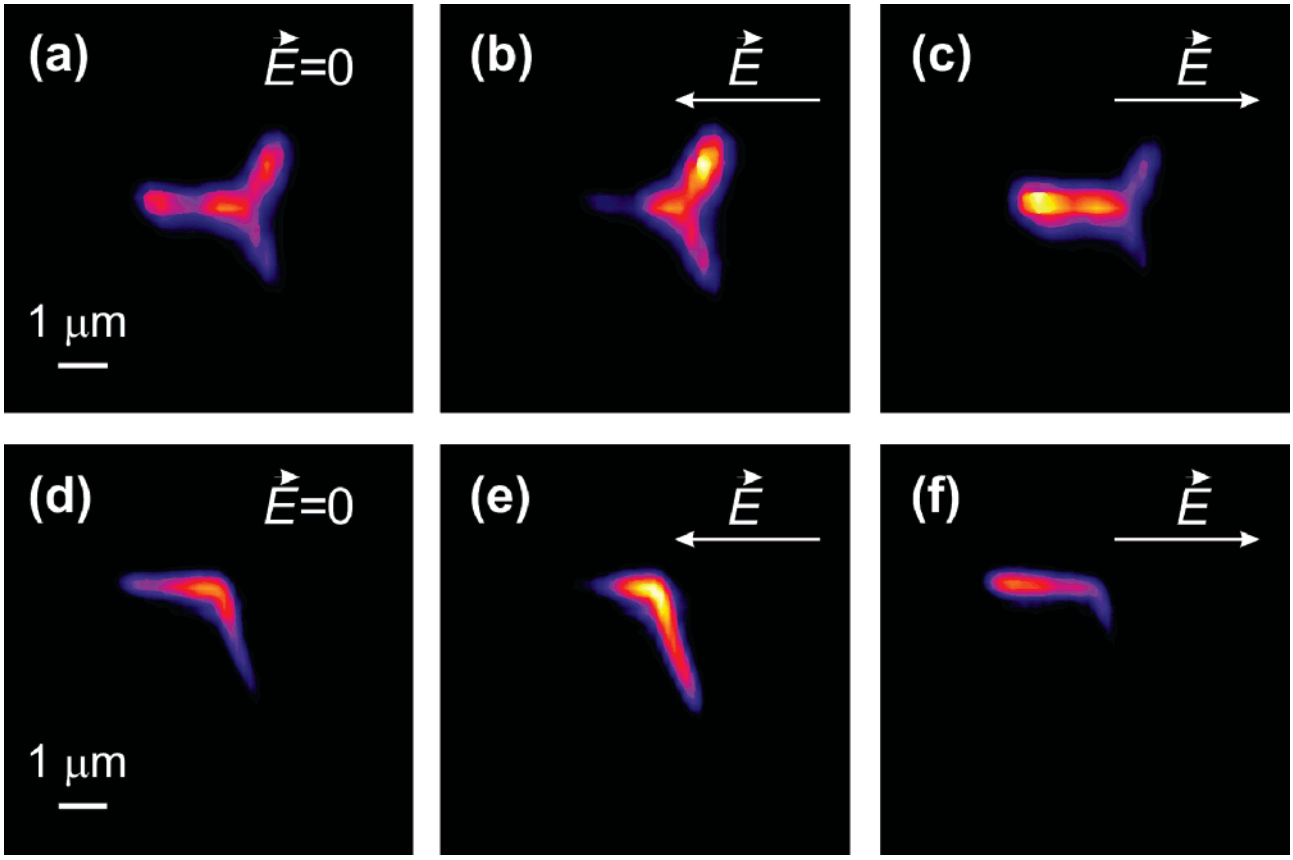

Figure 2. Effects of an external electric field on the emission from an isolated (a−c) tripod and (d−f) v-shaped NW under the following conditions: (a, d) no external field and (b, e) a negative and (c, f) a positive potential applied to the left electrode. Emission enhancement (quenching) is observed in the NW region closest (furthest) from the positive electrode.

emission intensity, as defined by the ratio of emission intensities with the electric field on versus off. In certain cases, increases near an order of magnitude are seen. At the same time, emission quenching occurs in opposite regions of the wire where the quenching factor is defined as a ratio of the NW emission with the field off versus on. Its magnitude is nearly identical to the emission enhancement for field strengths up to 20 kV/cm. Both effects are described below in more detail.

When the field polarity is reversed, the emission enhancement/localization "moves" to the opposite end of the wire closest to the (new) positive electrode. Figure 2a−c illustrates this effect for a tripod-shaped NW. In particular, between images b and c the field points in opposite directions. However, clear differences in the spatial position of the emission and its intensity relative to the zero-field case (Figure 2a) are apparent. In Figure 2b the emission is localized/enhanced on the right side of the wire, whereas, by contrast, in Figure 2c the enhancement/localization occurs on the left side of the wire. Another example for a v-shaped NW is shown in Figure 2d−f.

Repeated switching of the external electric field orientation causes cycling of the emission enhancement and quenching. This is illustrated in Figure 3 where emission intensities from specific regions of the wire are plotted as a function of time. In the particular case considered, points 1 and 2 show a ∼1.5-fold fluorescence enhancement/quenching during each half cycle of the modulated field. No electric field was applied during the first 20 s of the trajectory to obtain a baseline reference level. In the figure the electric field points from left-to-right or right-to-left. Similar enhancement/quenching trajectories are seen in other wires within the same image. An accompanying movie, illustrating the effect, is provided in the Supporting Information. When the external field is turned off, the NW emission redistributes itself over the entire wire. Subsequently, both spectral heterogeneity and emission intermittency are observed, as previously noted for single CdSe NWs.[19]

Emission Response to Electric Field Strength. Both the enhanced emission intensity and quenching behave nonlinearly with field strength. In the analysis, only components of the electric field parallel to the NW axis are considered for wires not perfectly aligned with the field. Results of the measurement for 12 single wires at the air/glass substrate interface are shown in Figure 4a (enhancement) and b (quenching). Experiments were conducted by slowly modulating the field between 0.01 and 0.5 Hz and comparing the maximum (or minimum) emission intensity to the zero-field value. These ratios then provide "pure" enhancement and quenching factors. A third-order polynomial fit is provided as a guide to the eye.

From both figures, below ∼20 kV/cm, the enhancement and quenching show similar field dependencies. Quenching slightly dominates enhancement. Above 20 kV/cm, the enhancement appears to saturate at 2.5 in contrast to the quenching which continues to increase. Higher field experiments are limited by the output of the high-voltage amplifier. In ref 19 we previously estimated the emission quantum yield (QY) of CdSe NWs to be approximately 0.1%. Since the current study uses analogous CdSe NWs we assume similar QYs here. A 2−3-fold fluorescence enhancement/quenching induced by external electric fields thus implies NW QYs of 0.2−0.3% (0.03−0.05%) when

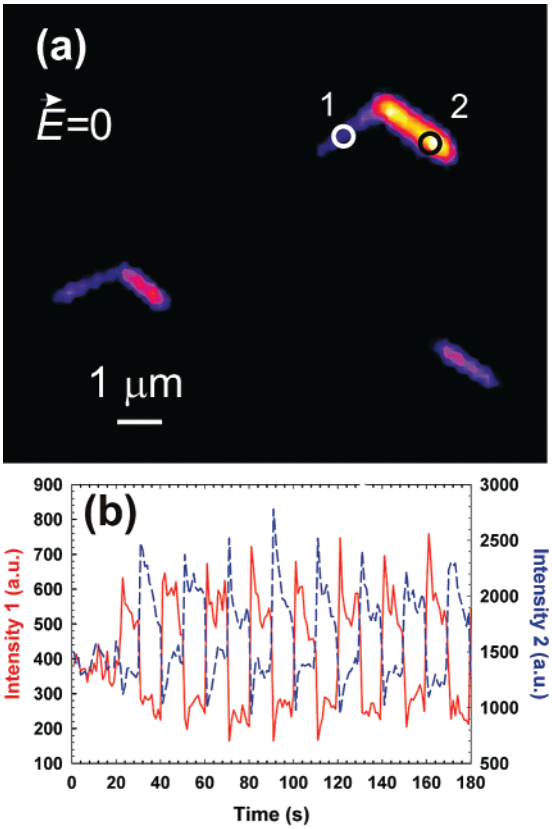

Figure 3. (a) Two v-shapes and a straight wire. (b) Plot of the intensity in locations 1 and 2 while a oscillating stepwise electric field (28 kV/cm amplitude) is applied from left to right and vice versa.

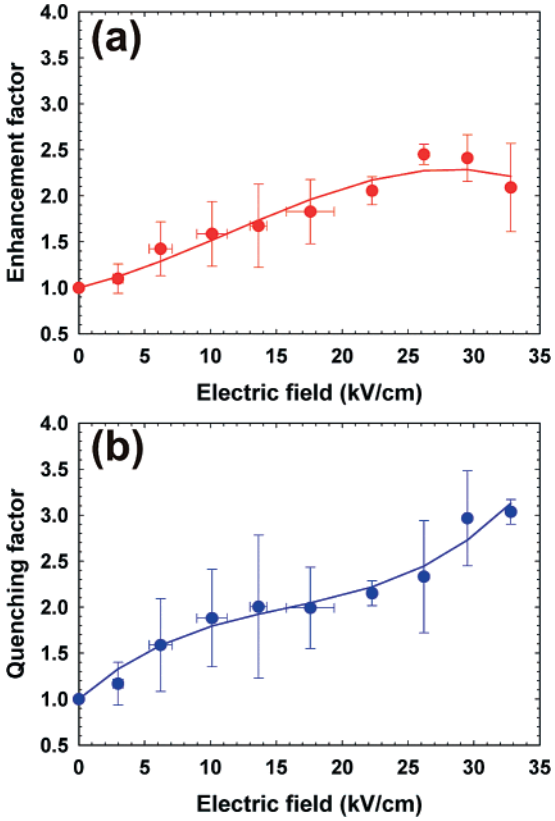

Figure 4. Field-induced (a) enhancement and (b) quenching factors averaged over 12 single NWs. Error bars represent a standard deviation.

enhanced (quenched). Furthermore, spectroscopic experiments performed on single wires exhibit a weak spectral dependence with electric field strength (Figure S2, Supporting Information). This insensitivity is consistent with the low overall fields used, being significantly smaller that the 10^5 V/cm values employed in actual Stark measurements.[9]

Stability of the Effect. Interestingly, the field-induced emission enhancement/localization for NWs at the air/glass interface is metastable. Specifically, under a constant electric field, the enhanced NW emission eventually redistributes itself over the entire wire during the course of several seconds. This can be seen in Figure 5, where images of a straight NW under zero-field conditions (Figure 5a) as well as under a constant electric field at two different times are shown (Figure 5b and c). From Figure 5c it is apparent that over the course of several seconds, the emission redistributes itself over the entire length of the wire despite the constant electric field. The emission intensity thus becomes comparable to that of the zero-field case. This can be seen also in Figure 3b where, on applying an electric field, the emission intensity changes sharply and within a few seconds relaxes to near zero-field intensities. An additional movie illustrating this effect is provided in the Supporting Information. The intensity heterogeneity and intermittency reported previously for NWs under zero-field conditions[19] are still present here under moderate field strengths. This can be seen through the nonuniform emission intensities along the NW length in Figure 5a−c.

Frequency-Dependent Response. At low frequencies the metastable NW emission includes a fast intensity response to reversals of the electric field direction. This is accompanied by eventual relaxation of the intensity to the zero-field level over the course of several seconds. The varied behavior suggests phenomena governed by different physical processes. Measurements of the NW emission intensity modulated by ac electric fields were therefore conducted. We found that the enhancement/quenching effect at a given field strength persists up to 500 kHz. This is illustrated in Figure 5d for experiments carried out with $E = 22.0$ ($\sigma = 7.9$) kV/cm. Since the data are recorded with a CCD using typical integration times of 0.1−10 s, many switching events occur during a given frame. As a consequence, the effective enhancement is analyzed differently from the previous Emission Response to Electric Field Strength section.

At low frequencies (0.01−0.5 Hz; typical acquisition time per frame 0.1−0.5 s) movies are analyzed by evaluating the average emission intensity (I_{mean}) from a given point of the wire over all frames. This value contains contributions from periods where the NW emission is enhanced and periods where it is quenched. To determine the net effect of the field, I_{mean} is compared to the intensity at the same location under zero-field conditions, I_o (separate movie). The ratio I_{mean}/I_o then indicates a net enhancement of the NW emission when in the presence of an external electric field.

Because of relaxation, emission trajectories acquired during low-frequency (<1 Hz) modulation experiments show clear decays during a given half cycle (Figure 3b). The relaxation phenomenon therefore lowers estimated emission enhancement factors. If analyses of the emission enhancement are conducted using peak (not average) emission intensities, slightly higher enhancement factors are obtained (blue diamonds, Figure 5d). These numbers more closely approximate the pure enhancement values in Figure 4a.

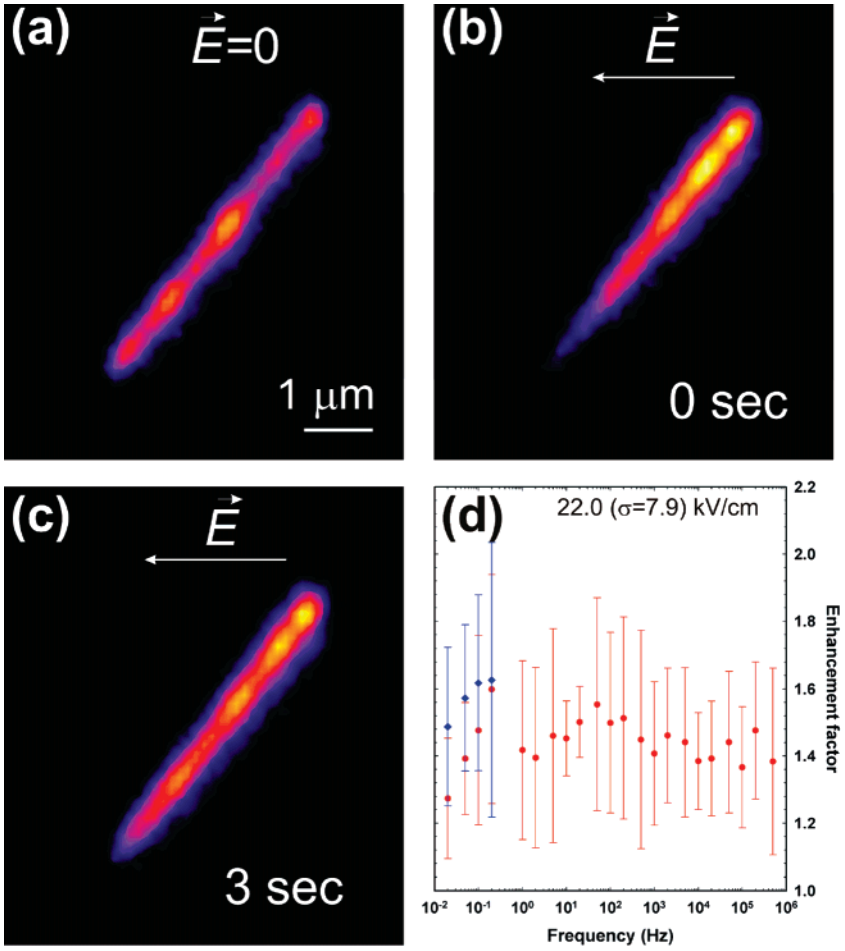

Figure 5. CdSe NW at the air/glass interface under (a) zero field, (b) field on, no delay, and (c) field on, 3 s delay conditions. Electric field: stepwise 14 kV/cm amplitude, 0.1 Hz. (d) Frequency response of the emission enhancement measured using a stepwise 22 kV/cm electric field. Blue diamonds were calculated without taking into account relaxation of the enhancement as discussed in the text.

At high frequencies (1 Hz to 500 kHz) the electric field switches on and off many times during a given frame (typical acquisition time 10 s/frame; field switching synchronized to the frame integration time). We therefore alternate sequences when the ac field is on and off. Off periods enable one to estimate I_o. Similarly, on periods provide I_{mean}. The ratio I_{mean}/I_o (obtained from the same movie) then reveals the overall effect of the external field, which is again a net enhancement of the NW emission.

Although Figure 4a and b shows that quenching slightly dominates enhancement, an overall emission enhancement is seen at all frequencies at the employed field strength [$E = 22.0$ ($\sigma = 7.9$) kV/cm]. This is because even when the polarity is reversed, the NW emission is never completely quenched (i.e., never goes to background levels; see Figure 3b for example) and the pure enhancement is approximately 2 at the considered field (see Supporting Information for more details). As a consequence, the net emission intensity in frames where multiple on/off cycles are averaged is enhanced. Corresponding enhancement factors between 1.3 and 1.6 are seen, which differ from the values of 2−3 in Figure 4a (identical field strengths) because the latter values consider the enhancement or quenching independently. Notably, the enhancement in Figure 5d does not change significantly over the range of frequencies investigated. This leads us to conclude that the field-induced enhancement/quenching persists up to 500 kHz or even higher since this is the cutoff frequency of our high-voltage amplifier. Finally, observations of fluorescence enhancement at 500 kHz suggest that the fluorescence enhancement/quenching build up and subsequent relaxation reflect two different physical processes. This is because their timescales differ by almost 6 orders of magnitude. In the former case, enhancements occur within 2 μs (a corresponding rate of 5×10^5 s^{-1}). By contrast, subsequent relaxation spans seconds (a corresponding rate between 0.1 and 1 s^{-1}).

NW Microelectrophoresis. Our working hypothesis is that mobile charges on or within the NW are responsible for the field-driven emission enhancement and spatial localization. In particular, mobile electrons are assumed to be responsible for the enhancement since the effect always occurs at the NW end closest to the positive electrode. Supporting this are estimates of the carrier mobility showing large values more consistent with the electron than with the heavier hole. Charged excitons are not considered due to their small room-temperature binding energy.[24] Furthermore, preliminary experiments conducted under applied electric fields, seeking to reveal potential exciton diffusion, show no increases of the emission line width beyond the diffraction limit.[24,25]

(24) Sanvitto, D.; Pulizzi, F.; Shields, A. J.; Christianen, P. C. M.; Holmes, S. N.; Simmons, M. Y.; Ritchie, D. A.; Maan, J. C.; Pepper, M. *Science* **2001**, *294*, 837.
(25) Nagamune, Y.; Watabe, H.; Sogawa, F.; Arakawa, Y. *Appl. Phys. Lett.* **1995**, *67*, 1535.

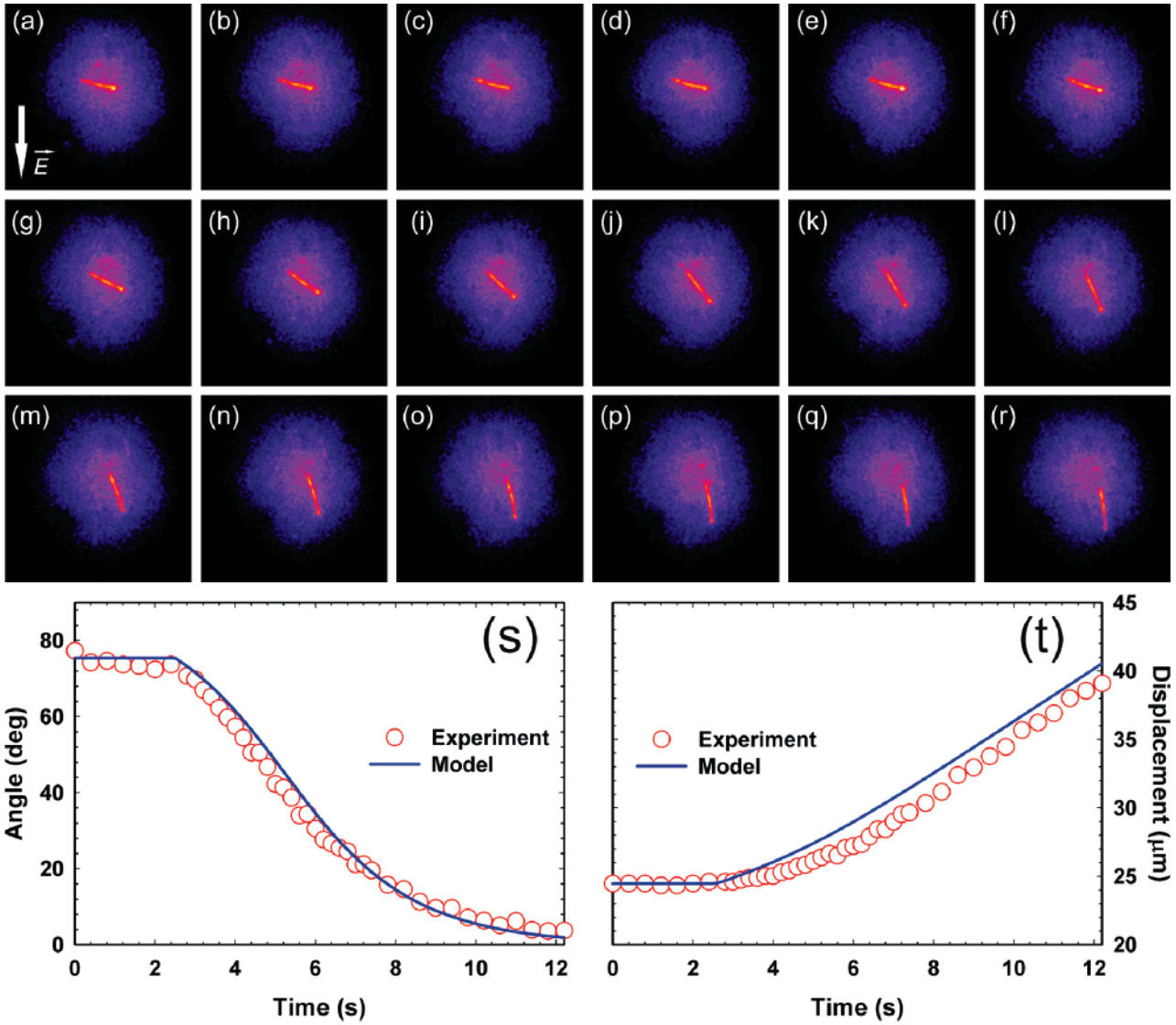

Figure 6. Montage of images (a−r) illustrating NW bundle rotational and translational dynamics in oleic acid after a 500 V/cm dc electric field has been applied between the third and fourth frames. Image size: 100 × 100 μm^2. Image acquisition time: 0.2 s. Time interval between images: 0.4 s. Temporal variation of the NW bundle (s) angle α and (t) position from the images. Solid lines are fits to the data using a model described in the text.

More details about the proposed mechanism are provided in later sections. However, here we directly test for the presence of such mobile charges through electrophoresis experiments. This is perhaps the simplest study that provides quantitative information about the magnitude and possible origin of stray charges. Experiments were conducted on NWs in toluene, chloroform, hexane, oleic acid, and immersion oil. Early studies involved NW ensembles, although it was ultimately concluded that such experiments provided only the sign and number of net *excess* charges on the NW. No information about the absolute number of mobile carriers present could be extracted given the possibility of charge compensation by mobile species of the opposite sign. The experiment did, however, suggest the origin of these unbound charges as will be described shortly.

To circumvent these limitations, microelectrophoresis experiments were conducted on small NW bundles in immersion oil or oleic acid. These experiments involved the use of an inverted microscope with a microcavity built atop a cover slip (Experimental Section). Wires were observed either under epi-illumination (i.e., through their emission) or under bright-field conditions. In epi-illumination mode, typical laser excitation intensities were 100−200 W/cm^2 with constant dc fields between 500 V/cm and 2 kV/cm. In all cases, single wire/bundle experiments showed that in either solvent the wires behaved as though positively charged. Moreover, the high viscosity of the solvent enabled an accurate recording of their dynamics. Nominal mobilities of 4×10^{-4}−10^{-3} μm/s/V/cm (10^{-3}−10^{-2} μm/s/V/cm) were seen for wires in immersion oil (oleic acid).

At the outset of these experiments, many wires do not happen to be oriented along the (eventual) direction of the applied electric field. Thus, when a potential is introduced, the wires first rotate to align themselves with the field. Figure 6a−r shows a series of frames from a movie illustrating NW rotational and translational motion in oleic acid. A full movie is provided in the Supporting Information. While this behavior can potentially be explained by the presence of internal dipoles due to the spontaneous polarization of wurtzite NW sections[26−28] the wires

(26) Li, L.-S.; Alivisatos, A. P. *Phys. Rev. Lett.* **2003**, *90*, 097402.
(27) Blanton, S. A.; Leheny, R. L.; Hines, M. A.; Guyot-Sionnest, P. *Phys. Rev. Lett.* **1997**, *79*, 865−868.
(28) Nann, T.; Schneider, J. *Chem. Phys. Lett.* **2004**, *384*, 150−152.

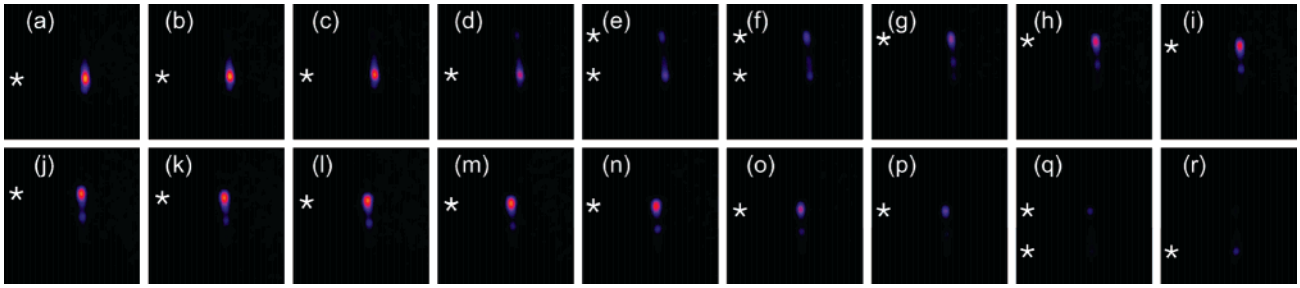

Figure 7. Straight NW bundle translating in immersion oil under a 2 kV/cm ac sinusoidal electric field (0.05 Hz). Image size: $16.8 \times 16.8\ \mu m^2$. Image acquisition time: 0.2 s. Time interval between images: 0.6 s. The asterisk is a guide to the eye showing the current spatial location of observed NW emission enhancement. Double asterisks indicate frames where the polarity of the field has switched and emission enhancement occurs at the opposite end of the wire.

eventually move toward the negative electrode, indicating an excess of positive charges.

These experiments also suggest that permanent dipoles are not responsible for the NW torque and subsequent field alignment. In this respect, NWs always align themselves by *minimizing* their angle with the electric field. By contrast, were a permanent dipole or a static distribution of positive and negative charges present, observed rotation angles should exceed 90° one-half of the time. This is because of the random orientation of wires in the channel prior to turning on the electric field. Furthermore, when the polarity of the field is suddenly reversed during an experiment, wires still rotate in the same direction. These results therefore rule out static dipoles and charges as the source of NW rotation and translation. The role of induced dipoles is also excluded since no NW translational motion should be observed in a uniform electric field. Instead, accumulation of mobile charges at either NW end is suggested as the cause of the phenomenon.

Furthermore, since NWs in oleic acid are positively charged and mobile electrons are thought to be responsible for the emission enhancement, an anticorrelation between the direction of NW electrophoretic motion and the spatial localization of its emission is expected. Figure 7 provides an example of NW translation in immersion oil with a slowly modulated ac electric field. Asterisks in the images show the position of the emission localization and enhancement. In the case where the field polarity is reversed (Figures 7 e,f,q) a second asterisk appears indicating the new NW region experiencing emission enhancement. In all cases, the effect occurs at the NW end opposite to the direction of its translation. Such observations suggest that even though both negative and positive charges exist on the NW surface, electrons are responsible for the emission enhancement/spatial modulation. These experiments also show that mobile carriers responsible for the effect reside on or within the NW since no substrate is involved in the measurement.

NW Translational and Rotational Model. To quantify the number of free carriers present we introduce a simple model for the NW rotational and translational dynamics. In our approximation, forces acting on the wire include electrostatic forces between unbound NW charges and externally applied electric fields as well as viscous forces from the fluid. For simplicity, no intrawire Coulomb attraction between carriers of opposite sign are considered. On applying an external electric field, mobile charges redistribute themselves on/within the NW and in many cases localize at opposite ends of the wire. Both a net charge due to a slight excess of one sign over the other and the corresponding torque due to the spatially separated carriers then force wires to rotate and translate in the fluid.

A set of equations describing both coupled motions is provided below. More details as to their origin can be found in the Supporting Information. The equations are

$$\frac{dx}{dt} = B(\alpha,L,d,\mu)|E|(Q_+ + Q_-) \quad (1)$$

and

$$\tau_\omega(Q_-,Q_+,L,d,\mu,E)\frac{d\alpha}{dt} = -\cos(\alpha)\sin(\alpha) \quad (2)$$

where the first describes NW translation and the second models their rotation. For simplicity we assume that the electric field points along the x axis. In either expression x defines the NW displacement, α is the angle between the NW axis and the electric field, μ is the fluid's viscosity, E is the electric field strength, and Q_+ (Q_-) is the charge magnitude on the NW end closer to the negative (positive) electrode. These latter values are desired parameters of the model since they effectively quantify the absolute number of mobile carriers present. Limitations exist though. Namely, the model provides only an estimate for the total number of mobile carriers present. It does not account for intrawire Coulomb interactions between charges.[29] Both the Supporting Information and ref 30 provide more details about the approximation. Explicit forms for B and τ_ω, which jointly depend on NW length (L), diameter (d), and solvent viscosity (μ), are also provided in the Supporting Information.

Several relevant parameters in eqs 1 and 2 can be estimated beforehand. Specifically, oleic acid has a dynamic viscosity of $\mu = 27.64 \times 10^{-3}$ kg/s m. Likewise, the electric field magnitude is typically $|E| = 500$ V/cm. The NW length (L) and diameter (d) can also be determined from optical and TEM experiments. In general, straight NWs used in these experiments form small bundles, consisting of approximately 3−8 wires. We therefore model such bundles by cylinders having the same total volume as all of the component wires put together. The equivalent diameter is $d = d_{single}\sqrt{n_{NW}}$ where d_{single} (~10 nm) is the diameter of a single NW and n_{NW} is the number of wires per

(29) Note that Q_+ and Q_- do not necessarily mean the absolute number of positive and negative charges present. While the subscripts indicate the net charge accumulated on the wire closest to the positive (Q_-) and negative (Q_+) electrode, in fact, attractive Coulomb interactions between more tightly bound electrons and holes potentially cause Q_- to reflect a net positive charge. This can be seen in Table 1. However, Q_+ and Q_- ideally represent the number of electrons and holes present.

(30) Cox, R. G. *J. Fluid Mech.* **1970**, *44* (4), 791−810.

Table 1. Parameters in the NW Bundle Translational and Rotational Model (n_{NW} 3−8)

L, μm	3.5	7.4	9.1	9.6	12.7
Q, e	38.4	30.0	41.1	68.1	78.9
Q_+	51.2	28.6	31.9	101.6	72.4
Q_-	−12.8	1.4	9.2	−33.5	6.5
Q_-/L (bundle density)	−3.6	0.2	1	−3.5	0.5
$Q_-/(L\ n_{NW})$ (single NW density)	−1.20 to −0.45	0.03 to 0.07	0.13 to 0.33	−1.17 to −0.44	0.06 to 0.17

bundle. In practice, this latter value is estimated from an analysis of the bundle's overall emission brightness as compared to the known emission intensity from single wires.

B and τ_ω in the model depend weakly on d and scale as 1/ln(L/d). Variations in these parameters yield only small changes in predicted translational (eq 1) and rotational (eq 2) speeds. To illustrate, for a typical wire with $L \approx 10$ μm and $d \approx 20-30$ nm, ln(L/d) $\approx 5.8-6.2$. Thus, a factor of 2 variation in diameter yields only discrepancies on the order of 10%. Similar behavior is seen with L. Its uncertainty arises from the ∼300 nm diffraction-limited optical resolution of the microscope. This translates into ∼3−6% variations of L (5−10 μm long NWs) and corresponding ∼4−8% variations in B and τ_w.

With these estimates in hand, eqs 1 and 2 can be fit to experimental data in order to extract values of Q_+ and Q_-. These are essentially the magnitudes of positive and negative charges localized on the NW ends.[29] Figure 6s and t shows experimental data (open circles) and accompanying fits (solid line) for the translational and rotational NW motion. Experimental values were obtained by analyzing movies such as the one in Figure 6. Best-fit parameters are provided in Table 1. Extracted values of Q_- vary from −33.5 to 9.2q ($q = 1.602 \times 10^{-19}$ C). In the most optimal case, corresponding single-wire charge densities, $Q_-/(Ln_{NW})$, range from 0.45 to 1.2 electrons per micrometer. In agreement with experimental observations, not only do mobile positive and negative carriers exist on or within the wire but also an excess of positive charges allows for the observed electrophoretic motion toward the negative electrode in oleic acid.

Calculated values of the linear charge density are lower limits to the true number. This is because the underlying model excludes attractive intrawire Coulomb interactions and implicitly assumes that all mobile carriers accumulate indefinitely at opposite ends of the NW. Clearly this is not physical due to the eventual Coulomb repulsion of like charges and in the opposite extreme partial compensation by oppositely signed species. Instead, what likely happens is that charges accumulate at NW ends distributed in such a way as to reduce their overall interaction potential energy. As a consequence, more charges are actually needed to produce the same torque, $T \approx L/2E(Q_+ - Q_-)$, experienced by NWs during rotational alignment. Supporting this are images such as those in Figures 2 and 5, which clearly show, through the emission, that field enhancement extends across a significant length of the NW. More detailed accountings of the actual NW charge distributions and attractive Coulomb interactions are therefore required if more precise Q_+ and Q_- values are to be obtained.

Two Sources of Mobile Charges. Where do these mobile charges come from? Two experiments provide clues for answering this question. Electrophoresis experiments, conducted in a variety of solvents, show that the sign and magnitude of net *excess* NW charges is solvent dependent. Wires in toluene behave as though negatively charged. Figure 8a is a color photograph of a NW ensemble in toluene prior to turning on a dc field. The wires are placed in a cuvette between two optically transparent indium−tin-oxide electrodes. Upon applying a dc field (∼300 V/cm), NWs migrate to the positive electrode. After a few minutes, a uniform NW coverage is obtained. Figure 8b is a color photograph of the resulting sample. Wires in oleic acid and immersion oil, by contrast, behave as though positively charged (see Figures S3, Supporting Information, and Table 1). This varied behavior suggests that some fraction of mobile charges originate from sources extrinsic to the wires, possibly due to (as of yet unidentified) charge-transfer events with impurities in solution.

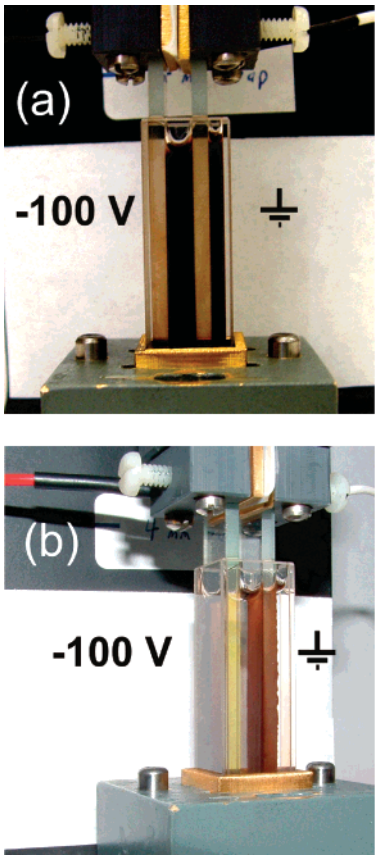

Figure 8. Color photograph showing an ensemble of CdSe NWs dispersed in toluene (a) before and (b) after applying a −100 V dc potential between two optically transparent indium−tin-oxide electrodes. The right electrode is grounded and at a higher potential relative to the left electrode.

Other sources of mobile carriers exist. In this respect we observed that the ac dielectrophoretic (DEP) alignment of CdSe[18] and CdTe NWs contains contributions from photogenerated carriers. Figures of aligned NWs are shown in Figure 9. By comparing the DEP alignment efficiency in the presence of 488 nm (2.54 eV, 100−200 W/cm^2) light versus under "dark" (i.e., ambient light) conditions we see that deliberately excited NWs move more quickly to the electrodes. Conversely, wires

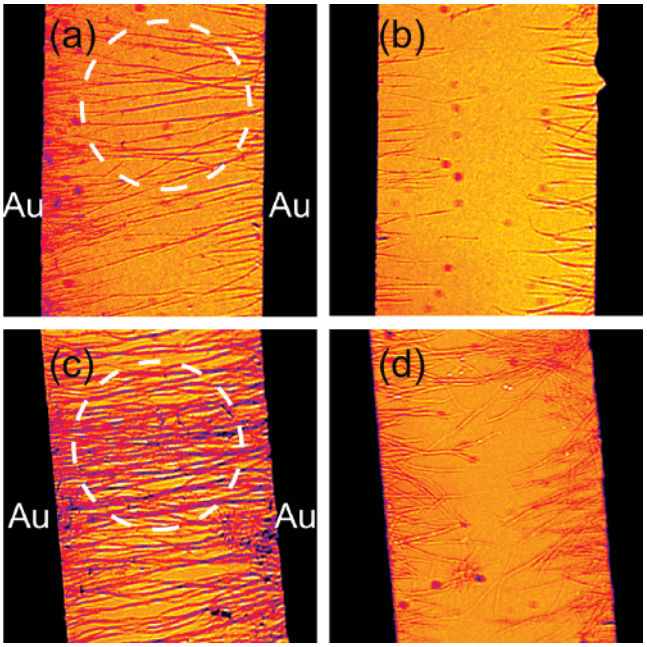

Figure 9. DEP alignment of (a) CdSe and (c) CdTe NWs in the presence of 488 nm light (~100 W/cm^2) centered about the dashed circle. DEP alignment of (b) CdSe and (d) CdTe NWs under ambient light conditions. Gap: 50 μm in all cases.

exposed only to ambient light show much slower, less efficient, DEP alignment. Because the operating principle of DEP involves interaction of field- and light-induced dipoles with electric field gradients,[18] these results suggest contributions to the overall NW mobility from (mobile) photogenerated carriers.

Apart from estimates of the total number of mobile carriers present (Q_+ or Q_-), it is difficult to definitively determine the fraction of charges that are solvent related versus those that are photogenerated. This is, in some part, due to limitations of the above electrophoresis experiments. More involved studies are thus required and likely involve trying to deliberately add charges to the NW surface through chemical means or by conducting NW electrophoresis experiments under different excitation intensities.

Postulated Origin of the Field-Induced Spatial and Intensity Modulation. We have now shown that mobile charges exist on or within solution-based CdSe NW. We have further shown that the spatial position of the NW emission as well as its intensity can be modulated using external electric fields. What remains to be done is to connect these two observations, linking the role of mobile carriers in inducing observed changes in NW optical properties.

The above electrophoresis experiments provide information about the absolute number of charges required to explain both translation and rotational NW dynamics. They do not, however, unambiguously indicate the location of these charges. This is identical to Millikan's experiment where observed charges could have been either on the surface or within the oil droplet. In either case, Gauss' Law applied to the dynamics of charged species prevents one from discerning their actual location.[31] As a consequence, we are free to place observed charges on or within the NW depending on the actual model proposed to explain the emission enhancement/localization. We favor the idea of surface-localized carriers for the following reasons.

It is known that stray mobile charges in the local environment affect the optical and electrical properties of nanostructures. For example, spectral diffusion in single colloidal QDs has been attributed to the random migration of NC surface charges causing time-dependent Stark shifts.[9] Furthermore, spectral diffusion and NC fluorescence intermittency (also called "blinking") appear to be connected.[10] The latter phenomenon is thought to be related to the sequential charging and discharging of individual QDs.[11,12] In either case, charges, possibly surface localized, play a role in the phenomenon.

Interestingly, the same behavior has been observed in individual solution-grown NWs. Specifically, solution-based CdSe NWs exhibit large intrawire spectral heterogeneities with average shifts of 62 ($\sigma = 27$) meV. Accompanying line widths of 103 ($\sigma = 22$) meV are also seen, inconsistent with lifetime-limited values.[19] Intrawire intensity fluctuations akin to fluorescence intermittency are likewise observed and exhibit near identical power law on/off kinetics.[19] This similarity to QD behavior, despite dissimilar electronic structures, suggests surface-localized charges as a point of commonality.

We therefore hypothesize the following. Mobile carriers exist on NW surfaces. They either originate through, as of yet unidentified, charge-transfer events or are photogenerated. The presence of such charges effectively passivates NW surface defect states and in turn changes the exciton nonradiative recombination rate. As a consequence photogenerated excitons in the vicinity of the localized carrier recombine radiatively. Passivated nonradiative decay channels likely relate to surface defects as supported by the low overall ensemble emission quantum yield (QY) of CdSe and CdTe NWs.[19,32] A cartoon schematic of this model is shown in Figure S4 of the Supporting Information.

In general, the effective passivation is local to the immediate vicinity of surface-bound carriers. However, applying an external electric field causes charges to migrate to opposite ends of the wire. The subsequent passivation of multiple electron acceptor states near the positive electrode causes the wire to become significantly brighter due to postulated changes in exciton nonradiative relaxation rates. For unknown reasons, no emission enhancement due to the presence of excess holes at the other end is observed.

The accumulation of charges at NW ends is not stable and likely leads to accumulation of counterions from a hydration layer present on the substrate under ambient conditions. This would suppress the effect of the external electric field, leading to near zero-field conditions and an eventual suppression of the enhancement/localization effect (Figure 5). In this respect, very preliminary studies to alter the NW environment show that wires embedded in polyvinyl alcohol exhibit a ~100-fold stability increase of the field-induced emission localization and brightening.

The frequency response of the average enhancement (Figure 5d) suggests carrier mobilities on the order of 0.04 cm^2/V s. These values are not consistent with the band transport of carriers. Furthermore, in principle, were carriers to be inside the NW Auger-mediated relaxation would likely increase, not

(31) Stratton, J. A. Electromagnetic Theory; McGraw Hill: New York, 1941; p 9.

(32) Kuno, M.; Ahmad, O.; Protasenko, V.; Bacinello, D.; Kosel, T. H. *Chem. Mater.* **2006**, *18*, 5722.

decrease, the nonradiative exciton decay rate.[33] Both provide the reasons for suggesting surface-localized carriers as responsible for the NW emission enhancement/localization. Finally, the larger mobilities of electrons (even if surface bound) relative to counterions in any hydration layer present rationalize the ~6 orders of magnitude difference between timescales for emission enhancement (<2 μs) and subsequent relaxation (seconds).

Two further scenarios are considered. In the first (a "state-filling" model) we posit that sufficient electrons and holes exist on the NW surface to occupy many, possibly all, surface defect states. Photogenerated carriers within the NW then find all nonradiative surface recombination pathways blocked and hence recombine radiatively. As a result, the overall NW QY increases. However, this hypothesis is not supported by the estimated linear charge densities of mobile carriers determined from the above electrophoresis experiments. Even in the best of circumstances (considering that the former values are actually lower limits) such numbers are far from the likely number of possible defect sites on NW surfaces.

In a second scenario we speculate that a few mobile electrons effectively passivate regions of the NW surface through the Coulomb repulsion of like charges. When coupled to their mobility, significant sections of the NW surface can therefore be passivated using only a few carriers. The picture is therefore, in many ways, an "electrostatic blockade" model for preventing carriers inside the NW from accessing nonradiative decay channels related to surface defects. Precedence for this hypothesis exists. Namely, the proposed scenario is virtually identical to a model developed by Maenosono to explain the fluorescence brightening of close-packed CdSe QD films.[13] In either the current study or Maenosono's earlier work a more quantitative model for the Coulomb passivation is needed. Furthermore, it is clear that more detailed studies identifying the origin, energy, as well as lifetime of long-lived surface (charge) trap states are required. However, the postulated mechanism would seem to be the simplest model for self-consistently explaining all of the presented data. It involves mobile charges. It further invokes surface carriers, avoids competing Auger effects, and ties into previous observations of intrawire NW spectral heterogeneity and intensity fluctuations. Most importantly, the model requires few not many charges to explain the effective passivation of the NW surface in agreement with direct electrophoresis experiments to quantify their number.

Possible Connection to NW Emission Intermittency. Continuing along these lines, a potential link likely exists between the observed field-induced emission enhancement/localization and apparent NW emission intermittency. Namely, we speculate that in the absence of external fields the same mobile carriers perform a random trap-to-trap walk on the NW surface. As a consequence, both the local electric field in and around the NW as well as its effective surface passivation fluctuate with time. This would then induce local changes in the NW QY causing apparent emission intermittency as shown in Figure 10. In the particular case considered, the emission intensity measured from the circled region exhibits near 100% changes as seen through an emission trajectory in Figure 10b.

If we consider NW intensity fluctuations as a noise originating from the random migration of surface-localized carriers, a complimentary estimate for their linear density can be evaluated through the measured signal-to-noise (S/N) ratio. In particular, if the S/N ratio at a given point is proportional to $\sqrt{N}$, where N is the number of mobile electrons within a diffraction-limited spot (~300 nm), the number of carriers responsible for the intensity fluctuations can be estimated. Since S/N = 1 at any given point in Figure 10b, the above shot noise analysis yields approximately one mobile electron per ~300 nm length. The corresponding linear charge density is then ~3 electrons per 1 μm length. This extracted charge density is ~3 times higher than numbers obtained from above electrophoresis studies (Table 1). However, they are comparable since previous electrophoretic numbers are actually lower limits to the true charge density.

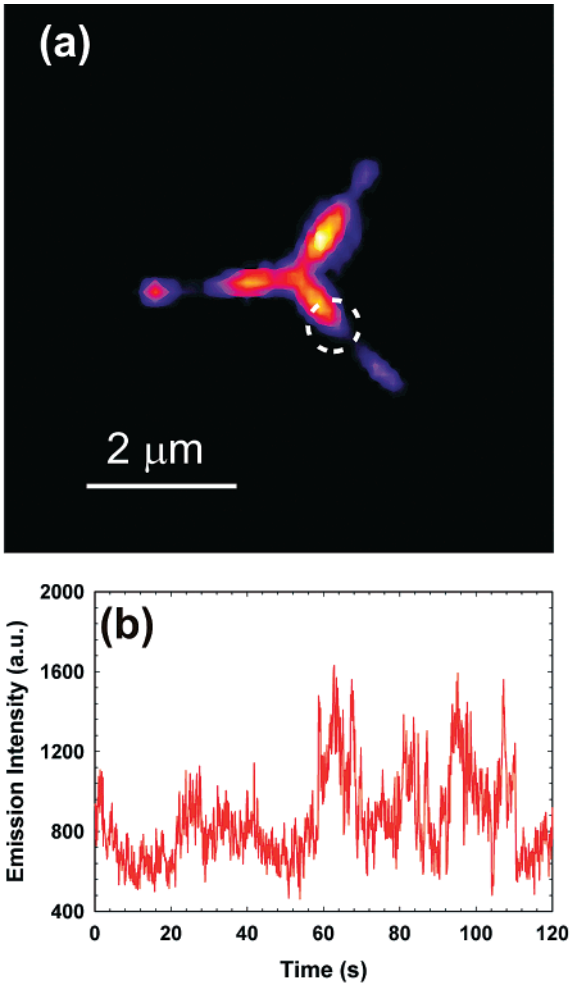

Figure 10. (a) CCD image of a single CdSe tripod. (b) Complementary emission intensity trajectory from the circled region.

Conclusions

In this study we discussed the possible role of mobile charges in explaining unusual optical properties of individual CdSe NWs when in the presence of external electric fields. Specifically, we observe both the spatial and the intensity modulation of NW emission using external ac or dc electric fields. Wires become bright in regions close to the positive electrode with an apparent 2−3-fold emission enhancement. The presence of mobile charges, thought to be responsible for the effect, is confirmed through direct ensemble and single NW/bundle electrophoresis experiments. Quantitative analyses of their rotational and translational dynamics yield lower limits to the linear charge

(33) Robel, I.; Bunker, B.; Kamat, P. V.; Kuno, M. *Nano Lett.* **2006**, *6*, 1344.

density. Resulting single-wire best-case values range from 0.45 to 1.2 per micrometer (for electrons). Although uncertainty exists as to the actual origin of these charges, we speculate that it arises from sources extrinsic to the wire as well as from additional contributions that are photogenerated.

Underlying our physical model is the modification of NW QYs due to the presence of surface-localized carriers. We suggest that the presence of such charges leads to electrostatic passivation of large regions of the NW surface due to the Coulomb repulsion of like charges. The proposed electrostatic "blockade" model then leads to local increases in the emission quantum yield due to changes in exciton nonradiative recombination rates.

The effect is most prominent when external electric fields maximize the concentration of carriers at a given end of the wire. However, it should be present under zero-field conditions as well. As a consequence, these observations of field-induced emission enhancement/localization raise further questions about the origin of recently reported NW emission intermittency.[19] Within the context of the current study, we suggest that under zero-field conditions, the same mobile surface charges can undergo a random walk between surface trap states. Local, time-dependent changes in the NW emission QY occur and result in characteristic intensity fluctuations. Such a model (once quantitative) may ultimately have broader applicability to other systems such as colloidal QDs given the ubiquity of stray charges. This highlights the importance of better understanding the interplay between external carriers and the intrinsic optical and electrical properties of nanostructures.

Acknowledgment. We thank Dan Meisel and Pavel Frantsuzov for a critical reading of this manuscript. We thank Jay Giblin for proofreading the text. We also thank Diana Hou for assistance in fabricating the interdigitated electrodes. M.K. thanks the University of Notre Dame, the NSF CAREER program (CHE-0547784), the NSF NIRT program (ECS-0609249), the Notre Dame Radiation Laboratory, and the DOE Office of Basic Energy Sciences for financial support as well as access to their equipment and facilities. M.K. is a Cottrell Scholar of Research Corporation.

Supporting Information Available: Model for NW translational and rotational dynamics, frequency-dependent field effect, cartoon schematic of microelectrophoresis substrates consisting of glass cover slips with microcavities glued to their top, NW emission spectra in the presence of an external electric field, NW electrodeposition in immersion oil, cartoon sketch illustrating the proposed model for NW emission enhancement, movies illustrating cycling of the fluorescence enhancement and quenching with applied electric field, movies illustrating short-lived emission enhancements at the air/glass interface, and movies of NW bundles undergoing rotation and translation in a microelectrophoresis experiment. This material is available free of charge via the Internet at http://pubs.acs.org.

JA073642W